18th International Conference on Protection & Automation in Power System
Shahrood University of Technology
January 9, 2024 - January 10, 2024

Design and Operation of Pulse Forming Network as Drive Circuit for Thomson Coil Actuator Used for High Voltage DC Circuit Breakers

Alireza Tabatabaei Malazi
Electrical Engineering Department
K. N. Toosi University of Technology
Tehran, Iran
a.tabatabaeimalazi@email.kntu.ac.ir

Seyed Hamid Khalkhali
Electrical Engineering Department
K. N. Toosi University of Technology
Tehran, Iran
Hamidkhalhali@email.kntu.ac.ir

Mohsen Taghizadeh Kejani
Electrical Engineering Department
K. N. Toosi University of Technology
Tehran, Iran
mohsen.t.k@email.kntu.ac.ir

Ali A. Razi-Kazemi
Electrical Engineering Department
K. N. Toosi University of Technology
Tehran, Iran
razi.kazemi@kntu.ac.ir

Alireza Jafari
Electrical Engineering Department
K. N. Toosi University of Technology
Tehran, Iran
a.jafari@email.kntu.ac.ir

Alireza Rezapoor Barabady
Electrical Engineering Department
K. N. Toosi University of Technology
Tehran, Iran
a.rezapoorbarabady@email.kntu.ac.ir

***Abstract*— Thomson coil (TC) actuators are well studied for ultra-fast disconnectors (UFDs) when fast operation is desired, such as for hybrid high voltage direct current circuit breaker (HVDC CB) applications used in HVDC transmission line protection. In this paper, a novel drive circuit using pulse forming network (PFN) for TC has been proposed. Comprehensive multi-physic finite-element simulations of PFN-powered TC are carried out to assess the effect of various current pulses on the TC electrical to mechanical energy conversion efficiency, compared with the efficiency obtained using the conventional single capacitor discharge approach. In this case, The TC is able to launch a 53-gram disk to a velocity of 9.4 m/s. Power for the TC is derived from a 13.06 J PFN comprised of forty 196 V electrolytic capacitors; the selected PFN-powered TC obtained efficiency of 17%, which is substantially greater than conventional capacitor-powered TCs with 5 % efficiency.**

Keywords- Thomson coil, Ultra-fast disconnector, High voltage direct current, Circuit breaker, Pulse forming network, Efficiency

I. Introduction

Further development and extension of HVDC and FACTS are being driven by the fast growth of power electronics and the pressing need to integrate remote large-scale renewable energy sources into the pure HVDC or interconnected HVAC/HVDC systems [1-4]. For HVDC, there are several technical and economic superiority over conventional HVAC power transmission, such as being able to use both long underground and submarine cables or long overhead lines to transfer enormous amounts of power over great distances with low loss [5-8] and asynchronous connections between AC systems with various frequency ranges [9]. These superiorities necessitate the development of multi-terminal HVDC systems [1]. Due to the low total line impedance of HVDC transmission links, which causes fault current to rise rapidly, utilizing an immediate detection and isolation of the faulted HVDC line is required for their protection [1, 10, 11]. Interruption is much more difficult for DC CB than it is for AC CB, because DC lacks zero-crossing, which aids fault isolation in the AC system [12]. DC CBs are generally classified into three categories: mechanical circuit breakers (MCBs), solid-state circuit breakers (SSCBs), and hybrid circuit breakers (HCBs) [13-16]. The HCB configuration benefits from the solid-state breaker's fast operation speed and mechanical breakers carrying high load current with low on-state losses [17-19]. HCBs typically contain three branches: a normal operation branch that includes a load commutation switch (LCS) and an UFD; a main breaker branch comprised of

several power electronic switches (often IGBTs); and an energy dissipation branch made up of surge arresters [13]. Current flows through the normal operation branch of HCB while operating normally; upon receiving a tripping signal, the LCS will instantly block to commutate the fault current into the main breaker [2]. Simultaneously, the main breaker will be activated to provide a path for the fault current. Once the fault current completely commutates into the main breaker, the UFD will open under zero current [13]. To lower the rate of current rise (*di/dt*) during this time, a current limiting reactor (CLR) is employed [2]. Then, the main breaker will be turned off, and the surge arresters will dissipate the fault current [13]. Upon fault clearance, the residual current breaker (RCB) interrupts the flow of residual current and isolates the faulty line from the HVDC grid [20]. UFD is a fast mechanical switch [21] that has a decisive impact on determining HCB's interruption time [17]. UFD requires a quick mechanical operation, typically accomplished by utilizing a high-speed actuation mechanism. Hydraulic, pneumatic, linear motors, solenoid, magnetic, or spring-type actuation mechanisms require at least several milliseconds of opening time, which makes them unsuitable for DC breaking, while electromagnetic actuation mechanisms like TC may attain a sub-millisecond level of opening time [11]. For HCBs to operate quickly, an electromagnetic UFD model equipped with a TC actuator is required for system-level researches (transient stability, protection) and warranting proper operation of HCB. The optimization approach focuses on designing a PFN-feeding TC instead of a conventional capacitor bank, which must provide a high-value current pulse with an appropriate duration injected into the TC. To maximize the actuator's electrical-to-kinetic conversion efficiency, this investigation offers some design considerations for a fieldable PFN system. A Multiphysics FEM software called COMSOL has been used to simulate and validate the optimization process. The simulated UFD is intended to attain a minimum 10 mm open distance (equal to 30kv dielectric strength in air). Furthermore, it might be expanded to accommodate high-voltage applications.

II. TC Actuator Principle

The principle of a TC-based UFD's fast opening and closing operations will be described, and the main components are discussed as follows:

A. Structure and Mechanism of TC Actuator

Referring to Fig. 2, the four main parts of the TC-based UFD are: 1) interrupter; 2) TC operating mechanism; 3) energy storage and control unit; 4) damping and holding mechanism [22].

Fig. 3 illustrates the equivalent electrical circuit for the TC and the driver. When the voltage level of V_{tc0} is reached in the capacitor bank C_{tc}, switch S is opened to separate the driver from the power source. When the UFD must open, the thyristor S_{UFD} of the opening coil will be triggered by the external signal from DC grid protection. By activating this switch, the pre-charged capacitor bank is allowed to discharge through the opening coil

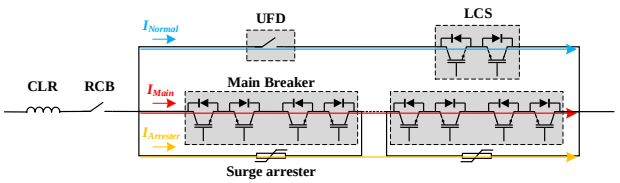

Figure 1. The structure of HCB.

by injecting a fast-rising discharge current pulse into the opening coil i_c as seen in Fig. 5 [17], an alternating magnetic field is created. This, in turn, causes a reverse-induced eddy current i_a to be generated on the disk [11] through mutual inductance M [17]. The induced current's direction and the resulting magnetic field creates a significant repulsive force between the coil and the disk [11]. As the coil is held firmly by its holder on a stationary frame, the disk together with the moving contact will be repulsed to move downward and open the contacts at a high speed. In this specific circuit, the diode restricts the rate at which the current decays once it has peaked. Activating a second switch that controls the discharge through the closing coil is how the closing action is carried out similarly. Then, the disk moves upward to close the contacts. Bi-stable springs with hold and latch mechanisms stop this movement. This spring absorbs some of the mechanism kinetic energy, thus damping the movement before reaching the stop [22].

B. Design of the TC Actuator

Fig. 4 shows the design variables of a TC, while TABLE I presents the parameter data for TC and its driver. The TC comprises 13 turns of enameled rectangular cross-section conductors in the dimension of 0.8×2.50 mm^2. The coil has an inner and outer radius of 6 mm and 24.1 mm, respectively, which are embedded in a holder, and fixed with epoxy resin. A

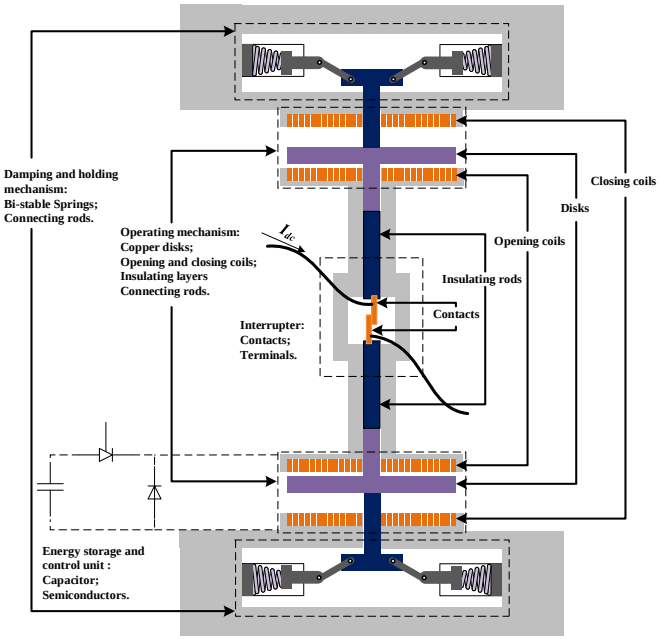

Figure 2. The main structure of UFD.

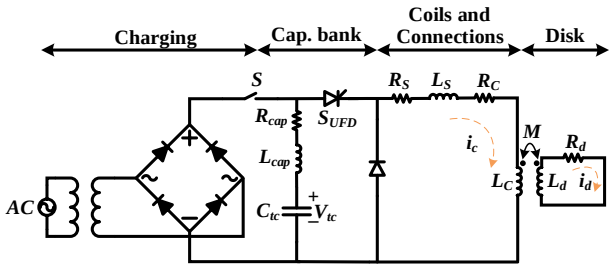

Figure 3. The equivalent electrical circuit of the TC and driver.

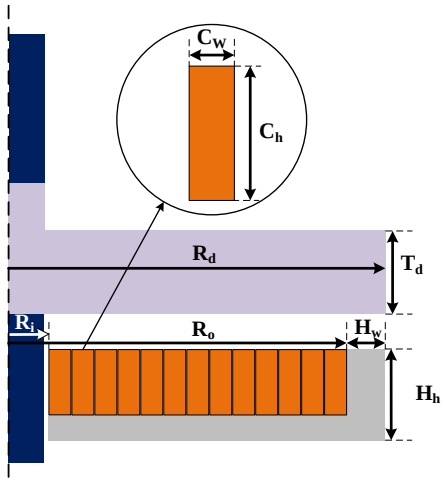

Figure 4. Simulated TC (coil, holder, and disk) dimensions.

repulsive disk with the mentioned dimensions in TABLE I is placed with a 0.1 mm air gap in the proximity of the coil.

C. Electro-dynamic UFD Model

1) Electrical Circuit Modelling: TC and Driver

The equations for the driving circuit and single-turn circuit are expressed as follows (1)-(2):

$$R_1 i_c + L_1 \frac{di_C}{dt} - \frac{d(Mi_d)}{dt} = V_{tc} \quad (1)$$

$$R_d i_d + L_d \frac{di_d}{dt} - \frac{d(Mi_c)}{dt} = 0 \quad (2)$$

$$R_1 = R_C + R_S + R_{Cap},\ L_1 = L_C + L_S + L_{Cap}$$

R_C, R_S, R_{Cap}, and R_d are the primary coil resistivity, stray resistivity of the connections, the capacitor resistivity, and disk resistivity, respectively, L_{Cap}, L_s, L_c, L_d, and M are the capacitor inductance, stray inductance, coil inductance, disk inductance, and mutual inductance, respectively [17]. The stored electrical energy in the capacitor bank is as follows:

$$E_{Cap} = 0.5 C_{tc} {V_{tc}}^2 \quad (3)$$

2) Dynamic Mechanical Model

TABLE I. TC AND DRIVER DESIGN PARAMETERS

parameter	Data	parameter	Data
Coil outer radius (R_o)	24.1 mm	Coil width (C_w)	0.8 mm
Coil inner radius (R_i)	6 mm	Coil height (C_h)	2.5 mm
Disk thickness (T_d)	10 mm	Holder height (H_h)	7 mm
Disk radius (R_d)	25 mm	Holder width (H_w)	4.5 mm
Disk mass	53 g	Capacitor (C_{tc})	2 mF
Disk material	Aluminum	voltage (V_{tc})	250 V
Holder material	Carbon steel	Coil turn	13

The electromagnetic energy in this system (W_e) is made up of the stored energy in the coil, the disk and, the mutual inductance, which is expressed as:

$$W_e = \frac{1}{2} L_c i_c^2 + \frac{1}{2} L_d i_d^2 - M i_d i_c \quad (4)$$

The electromagnetic force between coil and disk is obtained by differentiating (4) [17]:

$$F_e = -\frac{dw_e}{dz} = \frac{dM}{dz} i_d i_c \quad (5)$$

The electromagnetic force is determined by the drive current, the eddy current, and the derivative of the mutual inductance between the drive coil and the disk [23]. The average velocity is as follows:

$$\bar{V} = \frac{\Delta z}{\Delta t} \quad (6)$$

Where Δz is the travel distance, and Δt is the travel time. The disk kinetic energy is as follows:

$$E_{kinetic} = 0.5 m \bar{V}^2 \quad (7)$$

Where m is the disk mass, and $\bar{V}$ is the average disk velocity.

D. Opening Operation

Due to the similarity of opening and closing operations, only the opening operation is examined in this article. Fig. 5 shows the results of opening operation with a 2 mF capacitor bank pre-

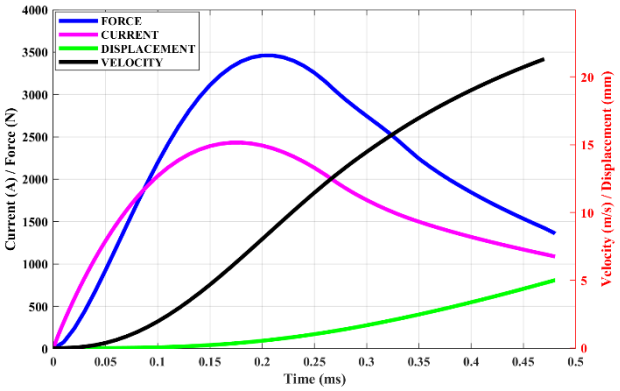

Figure 5. Simulation results for opening operation.

charged to 250 V, an approximately 2.4 kA current pulse is injected into the opening coil following the discharge of the capacitor bank, which accelerates the disk in the first milliseconds. The disk then travels at an approximately average velocity of 10.4 m/s.

E. Computation of TC Electrical Characteristics

The inductance of a single-layer spiral coil, in terms of dimensions in inches, can be computed according to (8).

$$L_c = \frac{a^2 n^2}{8a+11c}\ (\mu H) \tag{8}$$

$$a = 0.5(R_o - R_i), c = (R_o - R_i)$$

Where n, a, and c are the turn number of the coil, the average radius, and the thickness of the coil, respectively [24]. The resonance frequency of the L-C current source can be approximately calculated as [25]:

$$f_{res} = \frac{1}{2\pi\sqrt{L_c C}}\ (\text{Hz}) \tag{9}$$

Where L_C is calculated according to (8), and C is equal to C_{tc}. The coil's inductive reactance and electrical resistance can be computed according to (10) and (11), respectively:

$$X_c = 2\pi f L_c \tag{10}$$

$$R_c = \rho \frac{L}{A} \tag{11}$$

Where ρ, L, and A are coil material resistivity, length, and cross-sectional area, respectively. According to (10) and (11), the coil impedance can be written as (12):

$$Z_c = R_c + jX_c \tag{12}$$

F. TC Issues

1) Efficiency

A TC actuator must actuate the disk as quickly as feasible for a predetermined time period while ensuring the efficiency(η) of energy transfer from storage to motion [11]. In a capacitively driven TC, a large current pulse flows through the coil, and a significant amount of inductive energy is lost in the air gap between coil and disk. The energy initially stored in the electric field of the capacitor is divided into: (1) launch kinetic energy, (2) the joule heating of all subsystems, and (3) the residual energy stored in the electric and magnetic fields of the capacitors and inductors. Typically, only 5 % of the initial stored energy is converted to kinetic energy [26-28], although recent research; reports efficiencies as high as 14% for loaded mechanisms [26]. Reported capacitive system efficiencies have changed little over the last decade. Low efficiency indicates a high need for energy storage. The efficiency of the capacitively driven TC can be written as:

$$\eta_{Capacitor} = \frac{E_{kinetic}}{E_{Cap}} \times 100 \tag{13}$$

2) Maintenance and Reliability

Most TCs require several kilojoules of energy from capacitors, which are stored in millifarads of capacitance with kilovolts of pre-charged voltage. Such high-voltage, high-capacitance capacitors require particular care in their selection, implementation, and maintenance because high-capacitance capacitors tend to slowly degrade over time [11], which will reduce the capacitor's long-term reliability and lifetime. In addition, such a significant amount of energy might be highly hazardous for sensitive loads in a faulty condition [29]. These issues motivated research into designing, improving, and optimizing TC's driving circuit.

III. Pulse Forming Network (PFN)

PFNs are used to produce long, high-energy pulses, their limited stored energy and straightforward construction make them highly advantageous. Discrete capacitors and inductors combine to form the PFN, which is essentially an open-ended transmission line. The transmission line theory explains the process of discharging the PFN capacitors and creating pulses using PFN as a lumped model of a transmission line [29]. Various types of PFNs have been documented in [30]. In this paper, a PFN structure as an option for limited energy storage in pulsed power applications will be presented.

A. Input Data

The input data are the desired pulse width (T_P), rise time (T_r), amplitude of the current, number of sections (n), and load magnitude (see Fig. 6) [31].

B. Structure

The PFN power supply is shown in Fig. 7 schematically [29]. Starting with the input data and applying Guillemin's theo-

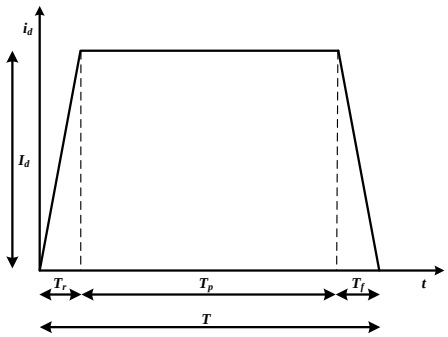

Figure 6. Required trapezoidal current pulse.

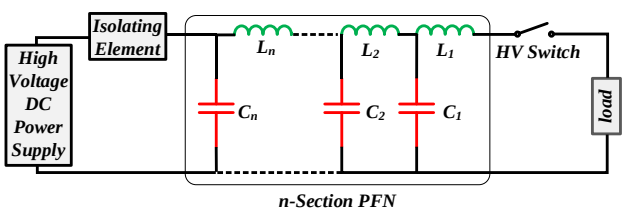

Figure 7. Block diagram of a PFN power supply.

ry the values of the capacitance and inductance of PFN sections (see Fig. 7) are calculated [31]. In the simplest type, the transmission line is simulated using equal L-C ladders. The characteristic impedance (Z_0) and pulse width for this PFN with n equal sections are expressed as [29]:

$$T_P = 2n\sqrt{LC} \tag{14}$$

$$Z_0 = \sqrt[2]{\frac{L}{C}} \tag{15}$$

Each cell's inductance and capacitance are represented by the letters L and C. It is possible to estimate the matched load ($R_L = Z_0$) pulse's rise time as [29]:

$$T_r = 0.8\sqrt{LC} \tag{16}$$

The stored energy in the PFN is as follows [29]:

$$E_{PFN} = 0.5ncV^2 \tag{17}$$

Where n is the sections number, C is each section's capacitance, and V is the charging voltage.

IV. PFN as Drive Circuit for TC

Most implementations of TC-based UFD, employ drive circuits that deliver a current pulse into the coil by discharging a capacitor bank, as shown in Fig. 3. This paper presents investigations on using PFN as a drive circuit instead of a conventional capacitor bank, as shown in Fig. 8.

A. Design Procedure

This research develops an analytical approach that expedites the optimization process, assuming that the TC has a linear equivalent resistance (R_L) equal to its impedance (Z_C); the nonlinearity of TC is ignored when determining its impedance. Therefore, the impedance (Z_0) is assumed constant in the calculation of the capacitance and inductance of PFN cells using equations (14)-(16) for this laboratory-scale simulated TC. One requirement for the PFN-powered TC is that its output current profile should be similar to its capacitor-powered TC. The charging voltage of PFN cells is determined by taking into account the resistive-inductive TC load characteristics and the desired current pulse characteristics. The initial charging voltage of PFN is modified after running the computer simulation several times until the desired current pulse profile is achieved. For optimum energy transfer in the main pulse, the PFN characteristic impedance (Z_0) is matched to the load impedance (Z_C).

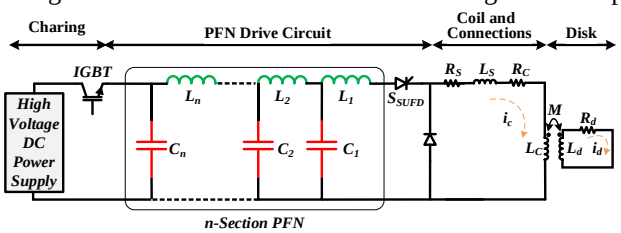

Figure 8. Equivalent circuit diagram of the proposed PFN-based power supply for TC actuator.

B. Efficiency

The PFN pulse-powered TC has demonstrated efficiencies considerably above the typical capacitor-powered 5 % efficiency. As a result, energy storage and prime power requirements would be decreased which are described below. The efficiency of the PFN power-supplied TC actuator can be written as:

$$\eta_{PFN} = \frac{E_{kinetic}}{E_{PFN}} \times 100 \tag{18}$$

V. Simulation

In this example, a model of a TC as a linear load will be presented. The TC is modeled by an inductor (L_C) and resistor (R_C), as shown in Fig. 9. The values of them were calculated according to (8) and (11), respectively. By calculating resonance frequency (f_{res}) according to (9), the coil's impedance (Z_C) is obtained according to (12). These calculated values are presented in TABLE II. The inductor and resistor account for the total effective inductance and resistance of the TC, which remain constant as the disk accelerates. The desired current pulse profile should have a 100 µs pulse width and 2.4 kA peak magnitude. In the characterization of the PFN to obtain the required current pulse, (1) the charging voltage value, (2) each section's calculated capacitance and inductance values according to (14)-(16), and (3) the required section number should be set as presented in TABLE III. Fig. 10 shows the equivalent schematic of the computed PFN power supply for TC.

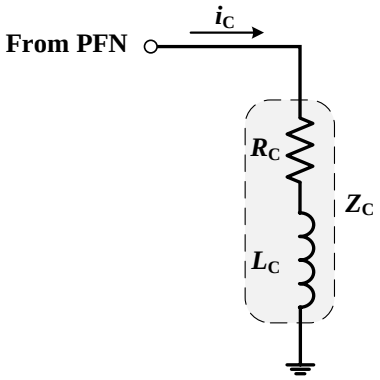

Figure 9. Representation of TC load.

TABLE II. CHARACTERISTICS OF TC

parameter	Data
TC resistance	15.76 mΩ
TC inductance	11.13 µH
TC impedance	71.75 mΩ
Resonance frequency	1 KHz

TABLE III. CHARACTERISTICS OF PFN

parameter	Data
Charge voltage	196 V
Each cell capacitance	17 µF
Each cell inductance	89 nH
Sections number	40

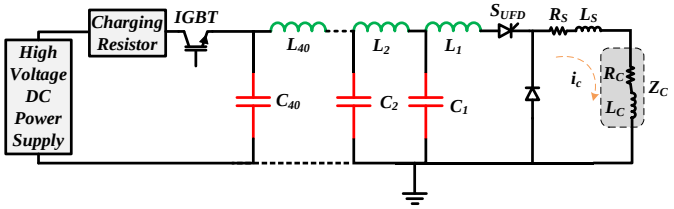

Figure 10. Final simulated Equivalent circuit diagram of a PFN power supply with 40 sections of *LC* units used for TC (L_1 to L_{40} are the inductors, and C_1 to C_{40} are the capacitors. Z_C is the matched load impedance).

A. *Results*

To evaluate the proposed structure, a PFN structure with the high voltage switch was simulated using MATLAB SIMULINK.

1) Current

Fig. 11 shows the PFN output current pulse predicted by the simulation. Fig. 12 shows the differences between the output current pulses with the nominal value of PFN elements and the output current pulse following the capacitor bank. There is a good agreement between the simulated PFN output current pulse and the capacitor bank discharge current pulse. Notice that in both of them, the peak current is approximately 2430 A.

2) Displacement and Average velocity

The black curve represents TC disk displacement supplied by a capacitor bank, while the red curve represents TC disk displacement supplied by a PFN. As demonstrated in the curves, supplying the TC by capacitor bank to reach the required 5 mm travel distance takes 0.48 ms, but supplying the TC in the same condition by PFN takes 0.53 ms. Therefore, according to (6), the average velocity ($\bar{V}$) for a capacitively powered TC is 10.4 m/s, and for a PFN-powered TC is 9.43 m/s.

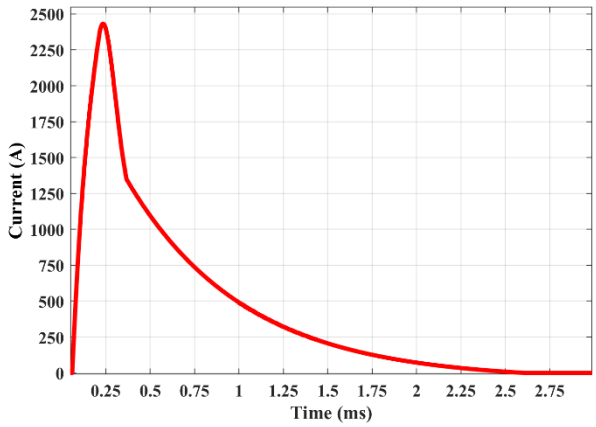

Figure 11. simulated output current pulse of the designed type B PFN injecting into the TC load.

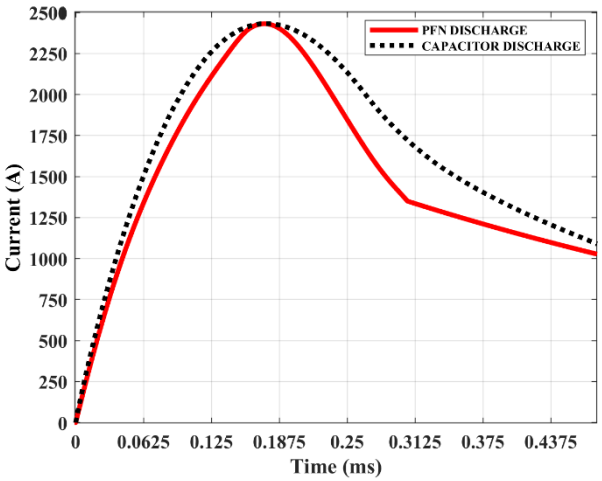

Figure 12. Comparison of the simulated output current pulse of the forty-section PFN and capacitor bank discharge with the same pulse flat top.

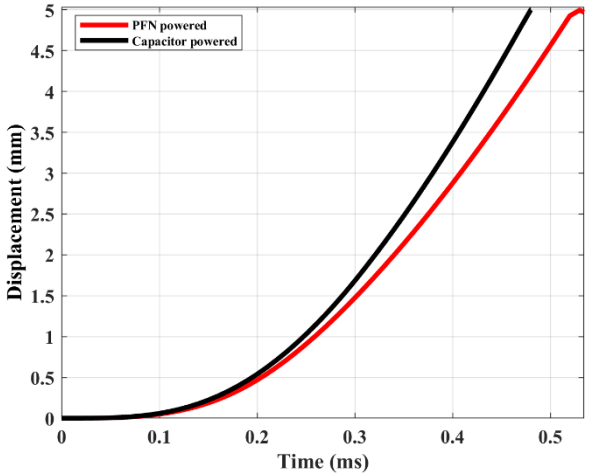

Figure 13. Comparison of the simulated displacement curve of a PFN-supplied and a capacitor bank-supplied TC.

According to (7), the kinetic energy (E_{Kinetic}) for a capacively powered TC is 2.86 J, and for a PFN-powered TC, it is 2.35 J.

3) Electrical-to-kinetic Conversion Efficiency

According to (17), the stored energy in the designed 40 sections PFN (E_{PFN}) with an initial voltage of 196 V is 13.06 J, while the stored energy for the same operation by a capacitor bank (E_{Cap}) according to (3) obtained 62.5 J. According to (13), efficiency for the mentioned capacitor bank power supplied TC ($\eta_{\text{Capacitor}}$) is obtained at 4.5 %, while according to (18), efficiency for the mentioned PFN power supplied TC (η_{PFN}) is obtained at 17.9 %, which shows 13.4 % efficiency improvement.

B. *Sensitivity Analysis*

To better understand how the various design parameters affect the actuator performance, a sensitivity analysis is conducted in this section. The following analysis concentrates

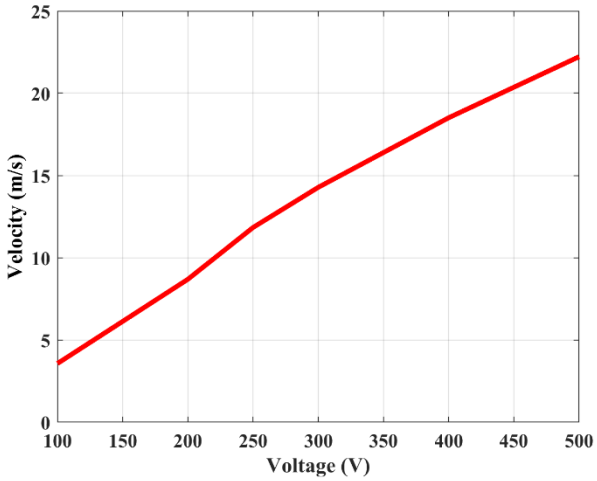

Figure 14. PFN charging voltage effect on average velocity.

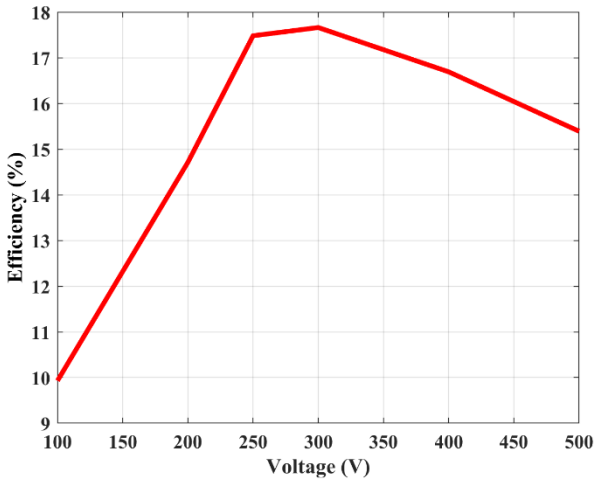

Figure 15. PFN charging voltage effect on efficiency.

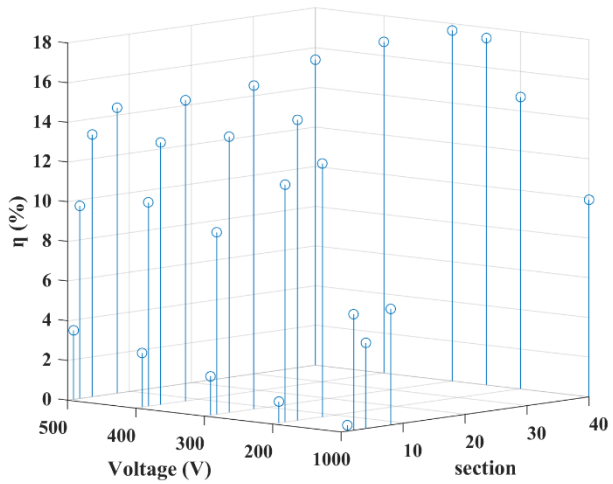

Figure 17. PFN sections number (n) and voltage (V) effect on efficiency (Ƞ) of a 100 µs current pulse width.

on the impacts of applying pulses with different widths, rise times, and voltages on the improvement of TC efficiency. During the assessment, one parameter is changed from a set of predefined values, while the rest remain constant. Based on the simulation results, a set of rules, related to the TC mechanical and electrical performance can be established.

1) Average Velocity Sensitivity to Charging Voltage Analysis

Fig. 14 shows the simulation results curve for the average disk velocity ($\bar{V}$) under different charging voltages of the designed 40-section PFN with 17µF capacitors and 89 nH inductors. As shown in Fig. 14, voltage has great effects on the velocity and velocity is increased by increasing the charging voltage.

2) Charging Voltage Sensitivity to Efficiency Analysis

Fig. 15 shows the simulation results curve for efficiency of the designed 40-section PFN with 17µF capacitors and 89 nH inductors suppling TC actuator under different charging voltages. As shown in Fig. 15, voltage has great effects on efficiency, and efficiency is increased by increasing the charging voltage, but as it can be seen this effect decreases for voltages greater than 300 V, this implies that voltages higher than 300 V are not reasonable.

3) Efficiency Sensitivity to Sections Number and Voltage

Fig. 17 is the summary plot of a PFN-supplied TC actuator simulation results obtained from the sensitivity analysis, showing efficiency (*Ƞ*) for different charging voltages (*V*) and PFN sections number (*n*) in a 100 µs current pulse width. It is revealed that the charging voltage (*V*) between 200-300 V for the PFN and increasing the sections (*n*) would be the optimal values for the PFN-powered TC-based UFD.

VI. Conclusion

This investigation has presented the theoretical results of a PFN-powered TC, and also examined the effects of increased efficiency and component scaling on PFN size for TC actuator. The PFN presented here is charged to 196 V and able to deliver a relatively desired current pulse for the nonlinear TC load. This minimizes the need for high-capacitance capacitors, allowing manufacturers to use less expensive capacitors in the drive circuit while meeting practical requirements. The simulated TC in this investigation accelerated a 53-gram disk to 9.4 m/s average velocity with a maximum efficiency of 17.6 %, which is the highest efficiency reported for this type of launcher and several times greater than conventional TCs at equivalent mass, size, and velocity. It is concluded that power supplying TC with PFN instead of a capacitor bank is an efficient method and worthy of development.

References

[1] F. Mohammadi et al., "HVDC circuit breakers: A comprehensive review," IEEE Transactions on Power Electronics, vol. 36, no. 12, pp. 13726-13739, 2021.

[2] S. Wang, C. E. Ugalde-Loo, C. Li, J. Liang, and O. D. Adeuyi, "Bridge-type integrated hybrid DC circuit breakers," IEEE Journal of Emerging and Selected Topics in Power Electronics, vol. 8, no. 2, pp. 1134-1151, 2019.

[3] D. Povh, "Use of HVDC and FACTS," Proceedings of the IEEE, vol. 88, no. 2, pp. 235-245, 2000.
[4] M. T. Kejani, S. H. Khalkhali, and A. A. Razi-Kazemi, "A New Approach on Condition Assessment of MV Switchgear Based on Thermal Evaluation," in 2023 31st International Conference on Electrical Engineering (ICEE), 2023: IEEE, pp. 904-909.
[5] I. I. Hussein, S. Essallah, and A. Khedher, "Comparative study of HVDC and HVAC systems in presence of large scale renewable energy sources," in 2020 20th International Conference on Sciences and Techniques of Automatic Control and Computer Engineering (STA), 2020: IEEE, pp. 225-230.
[6] K. Meah and S. Ula, "Comparative evaluation of HVDC and HVAC transmission systems," in 2007 IEEE Power Engineering Society General Meeting, 2007: IEEE, pp. 1-5.
[7] T. Halder, "Comparative study of HVDC and HVAC for a bulk power transmission," in 2013 International Conference on Power, Energy and Control (ICPEC), 2013: IEEE, pp. 139-144.
[8] M. T. Kejani, S. H. Aleyasin, A. Safaeinasab, and K. Abbaszadeh, "A new non-isolated single switch high step-up DC/DC converter based on inductor cells," in 2021 12th Power Electronics, Drive Systems, and Technologies Conference (PEDSTC), 2021: IEEE, pp. 1-5.
[9] Z. Yuan et al., "Research on ultra-fast vacuum mechanical switch driven by repulsive force actuator," Review of Scientific Instruments, vol. 87, no. 12, p. 125103, 2016.
[10] D. S. Vilchis‐Rodriguez, R. Shuttleworth, A. C. Smith, and M. Barnes, "Comparison of damping techniques for the soft‐stop of ultra‐fast linear actuators for HVDC breaker applications," The Journal of Engineering, vol. 2019, no. 17, pp. 4466-4470, 2019.
[11] M. Al-Dweikat, J. Cui, S. Sun, M. Yang, G. Zhang, and Y. Geng, "A review on Thomson coil actuators in fast mechanical switching," in Actuators, 2022, vol. 11, no. 6: MDPI, p. 154.
[12] B. Yin, X. Pei, X. Zeng, and F. Eastham, "A comparison between moving magnet and moving coil actuators for vacuum interrupters," in IECON 2019-45th Annual Conference of the IEEE Industrial Electronics Society, 2019, vol. 1: IEEE, pp. 5651-5656.
[13] G. Li, J. Liang, S. Balasubramaniam, T. Joseph, C. E. Ugalde-Loo, and K. F. Jose, "Frontiers of DC circuit breakers in HVDC and MVDC systems," in 2017 IEEE conference on energy internet and energy system integration (EI2), 2017: IEEE, pp. 1-6.
[14] P. Heidary, S. H. Khalkhali, M. T. Kejani, and A. A. Razi-Kazemi, "Design and Simulation of an Electromagnetic Actuator for a Linear Ultra-fast Disconnector (UFD) with Mechanical Stress Consideration," in 2023 27th International Electrical Power Distribution Networks Conference (EPDC), 2023: IEEE, pp. 136-141.
[15] S. H. Khalkhali, M. T. Kejani, and A. A. Razi-Kazemi, "Design of an Electromagnetic Actuator for a 2MW DC Circuit Breaker with a Fast Mechanical Switch Installed in the Railway Distribution Grid," in 2023 27th International Electrical Power Distribution Networks Conference (EPDC), 2023: IEEE, pp. 1-5.
[16] S. H. Khalkhali and A. A. Razi-Kazemi, "Design of a Combined Mechanical and Electrical Damper to Reduce Contact Speed at the Moment of Collision at the Endpoint," in 2022 13th Power Electronics, Drive Systems, and Technologies Conference (PEDSTC), 2022: IEEE, pp. 328-333.
[17] M. Zaja, A. A. Razi‐Kazemi, and D. Jovcic, "Detailed electro‐dynamic model of an ultra‐fast disconnector including the failure mode," High Voltage, vol. 5, no. 5, pp. 549-555, 2020.
[18] M. Hedayati and D. Jovcic, "Low voltage prototype design, fabrication and testing of ultra-fast disconnector (UFD) for hybrid DC CB," in Proc. CIGRE B4 Colloq., 2017, pp. 1-6.
[19] D. Jovcic, M. Zaja, and M. H. Hedayati, "Bidirectional hybrid HVDC CB with a single HV valve," IEEE Transactions on Power Delivery, vol. 35, no. 1, pp. 269-277, 2019.
[20] M. Callavik, A. Blomberg, J. Häfner, and B. Jacobson, "The hybrid HVDC breaker," ABB Grid Systems Technical Paper, vol. 361, pp. 143-152, 2012.
[21] A. Hassanpoor and J. Häfner, "Abb power grids hybrid hvdc breaker full-scale test: A breakthrough towards hvdc grid realization," in ABB, 2020.
[22] C. Peng, I. Husain, A. Q. Huang, B. Lequesne, and R. Briggs, "A fast mechanical switch for medium-voltage hybrid DC and AC circuit breakers," IEEE Transactions on Industry Applications, vol. 52, no. 4, pp. 2911-2918, 2016.
[23] Y. Zhou, Y. Huang, W. Wen, J. Lu, T. Cheng, and S. Gao, "Research on a novel drive unit of fast mechanical switch with modular double capacitors," The Journal of Engineering, vol. 2019, no. 17, pp. 4345-4348, 2019.
[24] H. A. Wheeler, "Simple inductance formulas for radio coils," Proceedings of the institute of Radio Engineers, vol. 16, no. 10, pp. 1398-1400, 1928.
[25] A. Kadivar, "Electromagnetic Actuators for Ultra-fast Air Switches to Increase Arc Voltage by Increasing Contact Speed," in 2019 International Power System Conference (PSC), 2019: IEEE, pp. 256-262.
[26] D. Vilchis-Rodriguez, R. Shuttleworth, and M. Barnes, "Finite element analysis and efficiency improvement of the Thomson coil actuator," in 8th IET International Conference on Power Electronics, Machines and Drives (PEMD 2016), 2016: IET, pp. 1-6.
[27] M. Barnes, D. S. Vilchis-Rodriguez, X. Pei, R. Shuttleworth, O. Cwikowski, and A. C. Smith, "HVDC circuit breakers–A review," IEEE Access, vol. 8, pp. 211829-211848, 2020.
[28] D. S. Vilchis‐Rodriguez, R. Shuttleworth, A. C. Smith, and M. Barnes, "Performance of high‐power thomson coil actuator excited by a current pulse train," The Journal of Engineering, vol. 2019, no. 17, pp. 3937-3941, 2019.
[29] S. Mohsenzade, M. Zarghany, M. Aghaei, and S. Kaboli, "A high-voltage pulse generator with continuously variable pulsewidth based on a modified PFN," IEEE Transactions on Plasma Science, vol. 45, no. 5, pp. 849-858, 2017.
[30] G.-H. Rim, E. P. Pavlov, H.-S. Lee, J. S. Kim, and Y.-W. Choi, "Pulse forming lines for square pulse generators," IEEE transactions on plasma science, vol. 31, no. 2, pp. 196-200, 2003.
[31] A. Musolino, M. Raugi, and B. Tellini, "Pulse forming network optimal design for the power supply of EML launchers," IEEE Transactions on Magnetics, vol. 33, no. 1, pp. 480-483, 1997.